International Journal of Railway Research, Vol. 4, No. 2, (2017), 41-56

Iran University of Science and Technology

International Journal of

Railway Research

ISSN: 2423-3838

Fuzzy Logic-Based Vector Control of Permanent Magnet Synchronous Motor Using Stacked Matrix Converter for Railway Traction Applications

Mahyar Khosravi [1], Seyed Saeed Fazel [2*], Vahid Abdollahi [3]

[1]School of Electrical Engineering, Iran University of Science and Technology, Tehran, Iran

[2]School of Railway Engineering, Iran University of Science and Technology, Tehran, Iran

[3]School of Electrical Engineering, Amirkabir University of Technology, Tehran, Iran

ARTICLE INFO

Article history:
Received: 21.09.2017
Accepted: 27.11.2017
Published: 14.12.2017

Keywords:
PMSM
Railway transportation
Vector control
Stacked matrix converter
Fuzzy supervisory control

A B S T R A C T

Recently, Permanent Magnet Synchronous Motors (PMSMs) have been widely accepted and employed in traction and railway transportation applications due to their various advantages such as small inertia, high efficiency and high torque density. In this research, in order to use these motors as traction drives in an effective way, the vector control scheme is used. In this strategy, the stator current is decomposed into 2 different components which are controlled separately. To increase the reliability of the system and also decrease the output voltage THD value, a multilevel inverter the so called Stacked Matrix Converter (SMC) is used in the power stage of the system. Also, to further improve the dynamic and steady state performance of the system in all different conditions, the conventional PID controllers that are used in the control scheme are trained by fuzzy supervisor controllers. Finally, for evaluating and validating the system performance in railway traction applications, the model of the system is simulated in MATLAB/Simulink environment and the results are analyzed.

1. Introduction

Since conventional railway systems use internal combustion engines, they suffer from low efficiency and also produce a large amount of air pollution. Hence, the electrified trains are considered as an attractive choice. In [1], a methodology is proposed for selection of the appropriate traction motor for different applications including railway transportation and it is concluded that the Permanent Magnet Synchronous Motor (PMSM) is superior to induction and wound-rotor synchronous motors for railway applications from different points of view such as efficiency, torque density, reliability, audible noise level and dynamic response. On the other hand, energy saving is an important issue for the railway system operators [2]. According to the high efficiency and torque density of the PMSMs [3] and also their energy recovery capability [4], these motors can provide further energy saving.

In several researches, PMSM design procedure, its comparison with other types of motors and the design requirements for railway transportation [5, 6] and hybrid Electric Vehicle (EV) [7] applications are discussed. In [8], the performance comparison between PMSMs with concentrated and distributed windings is done and it is concluded that when considering copper losses and power density, the concentrated

*Corresponding author
Email address: fazel@iust.ac.ir
http:// tlx.doi.org/……..

[Downloaded from ijrare.iust.ac.ir on 2026-11-16]

[DOI: 10.22068/IJRARE.4.2.41]

winding PMSM is better, while the distributed winding PMSM provides advantages such as better efficiency at high speeds, controllability, demagnetization tolerance and lower torque ripple.

On the other hand, the advancement of power electronic devices and converters has played an important role in the development of railway systems [9, 10]. This is due to the fact that simple and efficient control of AC motors is only possible by using power electronic converters such as inverters and rectifiers.

In recent decades, several strategies have been proposed for controlling AC motors. This is due to the increasing demand for fault-tolerant, reliable and high-performance electrical drives in different applications such as railway and ship transportation [11]. Several references have studied different methods for PMSM speed control. In [12], the control of instantaneous phase currents is used in order to control the PMSM speed. This method has some drawbacks such as obvious delay and generating flux current component. Moreover, the separate control of motor flux and torque is not possible using this method. In [13], a strategy called Most Torque per Ampere (MTPA) is proposed in order to achieve a higher power density, but using a look-up table is the drawback of this method since it needs a considerable amount of memory. In [14], a structure composed of two PMSMs connected to two Voltage Source Inverters (VSIs) is used for traction applications. When a fault occurs, this system can switch to the fault-tolerant mode by reconfiguration of the converter topology and separating the faulty leg.

In general, Field Oriented Control (FOC), Direct Torque Control (DTC) and sensor-less methods are three well-known strategies for controlling AC motors. The FOC method is an efficient strategy which is based on the decoupled control of torque and magnetic flux components [15]. In [16], the DTC and FOC strategies are applied to the PMSM and it is shown that DTC provides a better torque dynamic while FOC improves the steady state performance.

Several references such as [17-19] have studied sensor-less motion control strategies for PM motors in traction applications. These methods increase the reliability and also reduce the total costs due to the elimination of the sensors but rather complex calculations are needed since different estimation methods should be used.

In all the above mentioned references, the in use converter is a two-level bridge which generates more output harmonics and results in more voltage stresses on the switches compared to the multilevel converters.

Moreover, PID controllers are usually used in different loops of the control schemes that are used for controlling electric machines due to their simplicity. However, one of the main related issues is the appropriate tuning of the controller parameters. One of the approaches is using the Ziegler-Nichols method [20]. However, if the machine parameters are changed or a load variation occurs, the performance of the PID controller with constant coefficients won't be optimized. Therefore, the controller parameters should be continuously tuned during operation.

Fuzzy logic is a powerful theory which different controllers for numerous plants can be designed based on it. Fuzzy logic controllers have been successfully used for traction systems in [21, 22]. In [23], the fuzzy controller is used to generate the reference values of i_{sd} and i_{sq} for a PMSM. One of the main applications of the fuzzy logic theory is to design a supervisor controller for the conventional PID controllers in order to tune the PID controller parameters continuously hence, overcoming the aforementioned problems. This method has been used for DC motors [24] and also induction motors [25, 26].

In this paper, the stacked matrix converter is used in the vector control scheme that is used for a PMSM in traction applications. Using this multilevel converter will result in higher reliability and also decrease the voltage stresses on switches. It also decreases the THD value of the voltage applied to the motor and therefore, the torque ripple magnitude is reduced as well. Moreover, in this paper the fuzzy controller is used as a supervisor controller for tuning the conventional PID controller parameters.

2. PMSM and its Dynamic Modeling

The permanent magnet synchronous motor has been recently used in high-speed railway transportation applications [27]. For instance, the AVG permanent magnet traction motor

[Downloaded from ijrare.iust.ac.ir on 2026-11-16]

[DOI: 10.22068/IJRARE.4.2.41]

manufactured by Alstom can be considered. These motors are closed, self-ventilated and can reach a maximum speed of 4500 rpm.

The mathematical model of PMSM is expressed in the dq0 rotating frame attached to the rotor. The assumptions used here are as below [28]:

- The saturation effect is neglected.
- The eddy currents and hysteresis effects are neglected as well.
- The three-phase currents are balanced.

Equations (1)-(7) represent the dynamic model for this machine:

- Magnetic flux equations:

$$\psi_{sd} = L_{sd} i_{sd} + \psi_f \quad (1)$$

$$\psi_{sq} = L_{sq} i_{sq} \quad (2)$$

- Voltage equations:

$$v_{sd} = R_s i_{sd} + L_{sd} \frac{di_{sd}}{dt} - \omega_r L_{sq} i_{sq} \quad (3)$$

$$v_{sq} = R_s i_{sq} + L_{sq} \frac{di_{sq}}{dt} + \omega_r \left(L_{sq} i_{sq} + \psi_f \right) \quad (4)$$

- Electromagnetic torque equation:

$$T_e = \frac{3}{2} P \left(\psi_{sd} i_{sq} - \psi_{sq} i_{sd} \right) \quad (5)$$

- Mechanical equations:

$$J \frac{d\omega_m}{dt} = T_e - T_l - B\omega_m \quad (6)$$

$$\omega_r = P\omega_m \quad (7)$$

In (1)-(5), ψ_{sd}, ψ_{sq}, v_{sd}, v_{sq}, i_{sd} and i_{sq} are fluxes, voltages and currents of the motor represented in the d-q coordination, respectively. ω_r is the motor electrical angular speed and T_e is the electromagnetic torque. Also, ψ_f, p, R_s, L_{sd} and L_{sq} are the constant flux of the permanent magnet, number of the pole pairs, stator resistance and inductances, respectively. Finally in (6)-(7), J, T_L, B and ω_m are the motor and coupled load inertia, load torque, friction coefficient and motor mechanical angular speed, respectively.

The vector control strategy for this motor is described in the next section based on the above model.

3. Field Oriented Vector Control

It should be considered that field oriented vector control is generally the most popular strategy used for controlling AC Motors. In this paper, in order to achieve an appropriate dynamic performance, the Field Oriented Control (FOC) method is used as the control strategy of the traction PMSM. In FOC strategy, the stator current is decomposed into two components: the magnetic field current component and the torque current component. This is done by using dq0 transformation in which the resultant d and q components of the stator current are responsible for generating the flux and electromagnetic torque, respectively. Due to the presence of the constant flux of the permanent magnet, there is no need to produce any flux by means of i_{sd} and the reference value for this component would be zero as a result. Therefore, the stator current is decreased and the motor efficiency is increased as a result. These two components need separate control loops so that the flux and electromagnetic torque are controlled independently similar to a dc motor. By rearranging (5), (8) which demonstrates the relationship between the electromagnetic torque and the stator current components in the dq0 rotating frame, can be obtained:

$$T_e = \frac{3}{2} P \left(\psi_f i_{sq} + \left(L_d - L_q \right) i_{sd} i_{sq} \right) \quad (8)$$

If the i_{sd} value is considered zero in Eq. (8), then:

$$T_e = \frac{3}{2} P \psi_f i_{sq} \quad (9)$$

[Downloaded from ijrare.iust.ac.ir on 2026-11-16]

[DOI: 10.22068/IJRARE.4.2.41]

According to (9), the relationship between the electromagnetic torque T_e and i_{sq} is linear until the reference value for i_{sd} is kept zero. Therefore, a suitable dynamic response for T_e can be achieved through appropriate control of i_{sq}.

The structure of this control strategy includes the inner loops (for controlling the current components) and the outer loop (for controlling the speed). The block diagram of the FOC method is shown in Figure 1. It should be considered that in the block diagram depicted in Figure 1, the Stacked Matrix Converter (SMC) is used as the inverter. Also, the PI controllers are trained by the fuzzy supervisor controllers. The details are described in the next sections.

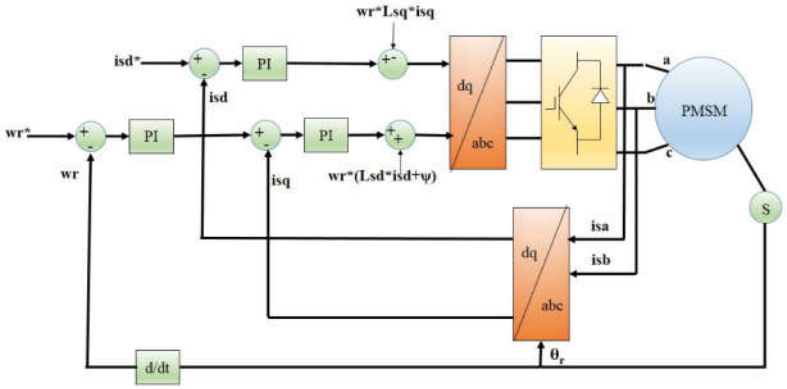

Figure 1. General block diagram of FOC strategy

4. Stacked Matrix Converter

There are several DC-AC converter topologies such as neural-point diode-clamped, flying capacitor and H-bridge inverters, matrix converters and cascaded inverters. Each of these topologies provides different features. The H-bridge inverter is the simplest and least expensive converter for AC motor drive applications in different power ranges. Therefore, this topology is usually used in different industrial applications, unless a new converter topology with obvious advantages compared to the H-bridge inverter is proposed for that specific application. The matrix converter structure is recently used by researchers in motor drive applications. The indirect matrix converter provides some advantages such as better voltage stability and lower THD value compared to other available converter topologies. Moreover, this converter provides output voltages with variable magnitude and frequency values. In this paper, the Stacked Matrix Converter (SMC) is used to drive the traction PMS motor. The topology of this converter is depicted in Figure 2. As it can be seen, this topology consists of three bidirectional switches in each phase. Employing bidirectional switches provides advantages such as generating zero-voltage-level with lower number of switches. The SMC also has other benefits such as variable output voltage magnitude and frequency. However, the presence of additional bidirectional switches makes the topology more complex and therefore, the control scheme is more complicated compared to conventional converters.

According to Figure 2, v_{AN} ,v_{BN} and v_{CN} are as (10)-(12):

$$v_{AN} = v_{AS} + v_{SN} \tag{10}$$

$$v_{BN} = v_{BS} + v_{SN} \tag{11}$$

$$v_{CN} = v_{CS} + v_{SN} \tag{12}$$

The three-phase load is considered to be balanced. Therefore:

$$v_{AS} + v_{BS} + v_{CS} = 0 \tag{13}$$

By combining (10)-(13):

[Downloaded from ijrare.iust.ac.ir on 2026-11-16]

[DOI: 10.22068/IJRARE.4.2.41]

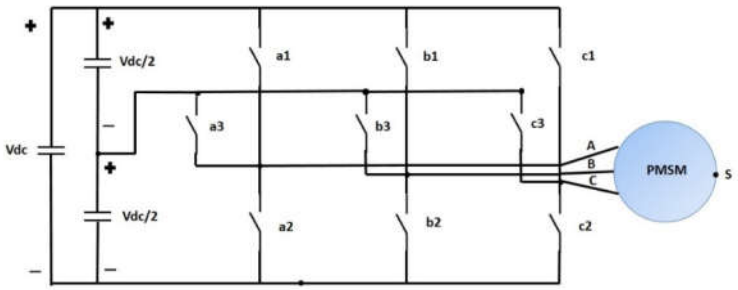

Figure 2. General block diagram of FOC strategy

$$v_{SN} = \frac{1}{3}\left(v_{AN} + v_{BN} + v_{CN}\right) \quad (14)$$

Therefore, the voltage of different load phases can be calculated by (15)-(17):

$$v_{AS} = v_{AN} - v_{SN} = \frac{2}{3}v_{AN} - \frac{1}{3}v_{BN} - \frac{1}{3}v_{CN} \quad (15)$$

$$v_{BS} = v_{BN} - v_{SN} = -\frac{1}{3}v_{AN} + \frac{2}{3}v_{BN} - \frac{1}{3}v_{CN} \quad (16)$$

$$v_{CS} = v_{CN} - v_{SN} = -\frac{1}{3}v_{AN} - \frac{1}{3}v_{BN} + \frac{2}{3}v_{CN} \quad (17)$$

Equations (15)-(17) can be written in the matrix form as shown in (18):

$$\begin{bmatrix} v_{AS} \\ v_{BS} \\ v_{CS} \end{bmatrix} = \frac{1}{3}\begin{bmatrix} 2 & -1 & -1 \\ -1 & 2 & -1 \\ -1 & -1 & 2 \end{bmatrix}\begin{bmatrix} v_{AN} \\ v_{BN} \\ v_{CN} \end{bmatrix} \quad (18)$$

According to the topology shown in Figure 2, the relationships between v_{AN} , v_{BN} and v_{CN} and the DC link voltage are as (19)-(21):

$$v_{AN} = \left(S_{a1} + \frac{S_{a3}}{2}\right)V_{dc} \quad (19)$$

$$v_{BN} = \left(S_{b1} + \frac{S_{b3}}{2}\right)V_{dc} \quad (20)$$

$$v_{CN} = \left(S_{c1} + \frac{S_{c3}}{2}\right)V_{dc} \quad (21)$$

Where S_{x_y} (x=a, b, c and y=1, 2, 3) are the switching states of different switches. If the switch is closed, the value will be $S = 1$; otherwise, $S = 0$.

As a result,

$$v_{AS} = \left[\frac{2}{3}\left(S_{a1} + \frac{S_{a3}}{2}\right) - \frac{1}{3}\left(S_{b1} + \frac{S_{b3}}{2}\right) - \frac{1}{3}\left(S_{c1} + \frac{S_{c3}}{2}\right)\right]V_{dc} \quad (22)$$

$$v_{BS} = \left[-\frac{1}{3}\left(S_{a1} + \frac{S_{a3}}{2}\right) + \frac{2}{3}\left(S_{b1} + \frac{S_{b3}}{2}\right) - \frac{1}{3}\left(S_{c1} + \frac{S_{c3}}{2}\right)\right]V_{dc} \quad (23)$$

$$v_{CS} = \left[-\frac{1}{3}\left(S_{a1} + \frac{S_{a3}}{2}\right) - \frac{1}{3}\left(S_{b1} + \frac{S_{b3}}{2}\right) + \frac{2}{3}\left(S_{c1} + \frac{S_{c3}}{2}\right)\right]V_{dc} \quad (24)$$

Based on (22)-(24), the output phase and line-line voltages generated by SMC can be calculated.

The different possible switching states of SMC are listed in Table 1. As an example, consider the forth row of Table 1 in which the switches a1, b3 and c3 are on, and the other switches are off. By using (19)-(21):

$$v_{AN} = \left(1 + \frac{0}{2}\right)V_{dc} = V_{dc}$$

$$v_{BN} = \left(0 + \frac{1}{2}\right)V_{dc} = \frac{1}{2}V_{dc}$$

$$v_{CN} = \left(0 + \frac{1}{2}\right)V_{dc} = \frac{1}{2}V_{dc}$$

[Downloaded from ijrare.iust.ac.ir on 2026-11-16]

[DOI: 10.22068/IJRARE.4.2.41]

Table 1. SMC different switching states

Switching States			Output Phase Voltages			Output Line Voltages		
Phase A	Phase B	Phase C	V_{AS}	V_{BS}	V_{CS}	V_{AB}	V_{BC}	V_{CA}
a1	b1	c1	0	0	0	0	0	0
a3	b3	c3	0	0	0	0	0	0
a2	b2	c2	0	0	0	0	0	0
a1	b3	c3	*Vdc/3*	*-Vdc/6*	*-Vdc/6*	*Vdc/2*	*0*	*-Vdc/2*
a3	b1	c3	*-Vdc/6*	*Vdc/3*	*-Vdc/6*	*-Vdc/2*	*Vdc/2*	*0*
a3	b3	c1	*-Vdc/6*	*-Vdc/6*	*Vdc/3*	*0*	*-Vdc/2*	*Vdc/2*
a1	b1	c3	*Vdc/6*	*Vdc/6*	*-Vdc/3*	*0*	*Vdc/2*	*-Vdc/2*
a3	b1	c1	*-Vdc/3*	*Vdc/6*	*Vdc/6*	*-Vdc/2*	*0*	*Vdc/2*
a1	b3	c1	*Vdc/6*	*-Vdc/3*	*Vdc/6*	*Vdc/2*	*-Vdc/2*	*0*
a2	b3	c3	*-Vdc/3*	*Vdc/6*	*Vdc/6*	*-Vdc/2*	*0*	*Vdc/2*
a3	b1	c3	*Vdc/6*	*-Vdc/3*	*Vdc/6*	*Vdc/2*	*-Vdc/2*	*0*
a3	b3	c2	*Vdc/6*	*Vdc/6*	*-Vdc/3*	*0*	*-Vdc/2*	*-Vdc/2*
a2	b1	c3	*-Vdc/6*	*-Vdc/6*	*Vdc/3*	*0*	*Vdc/2*	*-Vdc/2*
a3	b1	c2	*-Vdc/3*	*-Vdc/6*	*-Vdc/6*	*Vdc/2*	*0*	*-Vdc/2*
a2	b3	c2	*-Vdc/6*	*-Vdc/3*	*-Vdc/6*	*-Vdc/2*	*Vdc/2*	*0*
a1	b2	c2	*2Vdc/3*	*-Vdc/3*	*-Vdc/3*	*Vdc*	*0*	*-Vdc*
a1	b1	c2	*Vdc/3*	*Vdc/3*	*-2Vdc/3*	*0*	*Vdc*	*-Vdc*
a2	b1	c1	*-2Vdc/3*	*Vdc/3*	*Vdc/3*	*-Vdc*	*0*	*Vdc*
a2	b2	c1	*-Vdc/3*	*-Vdc/3*	*2Vdc/3*	*0*	*-Vdc*	*Vdc*
a1	b2	c1	*Vdc/3*	*-2Vdc/3*	*Vdc/3*	*Vdc*	*-Vdc*	*0*
a2	b1	c2	*-Vdc/3*	*2Vdc/3*	*-Vdc/3*	*-Vdc*	*Vdc*	*0*
a1	b3	c2	*Vdc/2*	*0*	*-Vdc/2*	*Vdc/2*	*Vdc/2*	*-Vdc*
a3	b1	c2	*0*	*Vdc/2*	*-Vdc/2*	*-Vdc/2*	*Vdc*	*-Vdc/2*
a2	b1	c3	*-Vdc/2*	*Vdc/2*	*0*	*-Vdc*	*Vdc/2*	*Vdc/2*
a2	b3	c1	*-Vdc/2*	*0*	*Vdc/2*	*-Vdc/2*	*-Vdc/2*	*Vdc*
a1	b2	c3	*Vdc/2*	*-Vdc/2*	*0*	*Vdc*	*-Vdc/2*	*-Vdc/2*
a3	b2	c1	*0*	*-Vdc/2*	*Vdc/2*	*Vdc/2*	*-Vdc*	*Vdc/2*

[Downloaded from ijrare.iust.ac.ir on 2026-11-16]

[DOI: 10.22068/IJRARE.4.2.41]

Next, the output phase voltages can be calculated using (22)-(24):

$$v_{AS} = \left[\frac{2}{3}\left(1+\frac{0}{2}\right) - \frac{1}{3}\left(0+\frac{1}{2}\right) - \frac{1}{3}\left(0+\frac{1}{2}\right)\right]V_{dc} = \frac{1}{3}V_{dc}$$

$$v_{BS} = \left[-\frac{1}{3}\left(1+\frac{0}{2}\right) + \frac{2}{3}\left(0+\frac{1}{2}\right) - \frac{1}{3}\left(0+\frac{1}{2}\right)\right]V_{dc} = -\frac{1}{6}V_{dc}$$

$$v_{CS} = \left[-\frac{1}{3}\left(1+\frac{0}{2}\right) - \frac{1}{3}\left(0+\frac{1}{2}\right) + \frac{2}{3}\left(0+\frac{1}{2}\right)\right]V_{dc} = -\frac{1}{6}V_{dc}$$

Finally, the output line-line voltages can be determined as below by using the output phase voltages:

$$v_{AB} = v_{AS} - v_{BS} = \frac{1}{2}V_{dc}$$

$$v_{BC} = v_{BS} - v_{CS} = 0$$

$$v_{CA} = v_{CS} - v_{AS} = -\frac{1}{2}V_{dc}$$

All the different voltages for different switching states shown in Table 1 can be calculated by a similar procedure like the above example.

The modulations used as the SMC switching scheme can be classified based on the switching frequency. Therefore, two modulation strategies can be considered: (a) square wave modulation (fundamental frequency switching), Pulse Width Modulation (PWM) (high-frequency switching).

The PWM itself can be implemented by two methods: Space Vector PWM (SVPWM) or Sinusoidal PWM (SPWM). In SPWM method, a high-frequency carrier waveform is compared with a fundamental frequency reference sinusoidal waveform. The frequency of this carrier waveform should be an integer 20 times more than the fundamental frequency [29]. In this paper, the SPWM strategy is used. Figure 3 depicts the gate signals generated by the SPWM method which are based on the switching states in Table 1.

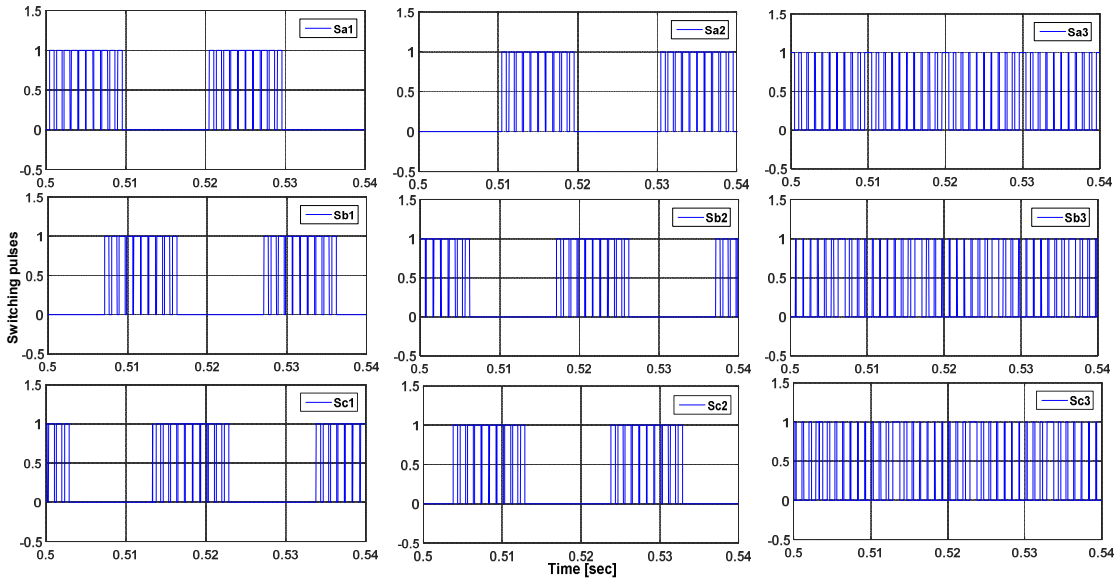

Figure 3. SMC gate signals

5. Fuzzy PID Supervisory Control

It is a common belief among control engineers that the dynamic performance of the system for different operating conditions can be improved if the PID controller gains are adjusted and trained in an appropriate way [30]. In this paper, the conventional PID controller parameters are trained by the supervisor fuzzy controller. Fuzzy logic can be considered as a mathematical theory that combines multivariable logic, probability theory and

[Downloaded from ijrare.iust.ac.ir on 2026-11-16]

[DOI: 10.22068/IJRARE.4.2.41]

artificial intelligence in order to use the knowledge of human experts. The fuzzy controller is basically a nonlinear adaptive controller which provides a robust performance for linear and nonlinear systems. Therefore, using the supervisor fuzzy controller can overcome disadvantages of the conventional PID controller such as unsatisfactory performance when the plant parameters or the operating conditions are changed. The transfer function of the PID controller is as (25):

$$G(s) = K_p + \frac{K_i}{s} + K_d s \quad (25)$$

In (25), K_p, K_i and K_d are the proportional, integral and derivative gains, respectively. By considering the error signal ($e(t)$) as the controller input, (25) can be written in another form as described in (26):

$$u(t) = K_p \left[e(t) + \frac{1}{T_i} \int_0^t e(\tau) d\tau + T_d \dot{e}(t) \right] \quad (26)$$

T_i and T_d are defined as (27)-(28):

$$T_i = K_p / K_i \quad (27)$$

$$T_d = K_d / K_p \quad (28)$$

Assume that the variation ranges of K_p and K_d are as (29)-(30):

$$K_p \in \left[K_{pmin}, K_{pmax} \right] \quad (29)$$

$$K_d \in \left[K_{dmin}, K_{dmax} \right] \quad (30)$$

Then, the normalized values of K_p and K_d can be described by (31)-(32):

$$K_p' = \frac{K_p - K_{pmin}}{K_{pmax} - K_{pmin}} \quad (31)$$

$$K_d' = \frac{K_d - K_{dmin}}{K_{dmax} - K_{dmin}} \quad (32)$$

Here, it is assumed that:

$$T_i = \alpha T_d \quad (33)$$

where α is the ratio of T_i to T_d .

For each conventional PID controller used in the motor control scheme, three fuzzy systems are designed. The inputs of all these systems are the error and error derivation signals. The outputs are K_p', K_d' and α . The first step in designing the fuzzy systems is to define membership functions in the variation ranges of all the input and output signals. Figures 4-6 depict these membership functions respectively. For the aforementioned fuzzy systems, the fuzzy rule bases are defined and then shown in Tables 2-4, respectively. It should be noted that the IF-THEN rules are defined according to the common knowledge about the PID controller performance and in such a way that in any condition, the best dynamic and steady state performances are achieved. For example, when the transient error has a high value, K_p and K_i should also have big values while K_d value should be small in order to get a better dynamic response. All the other rules can simply be obtained by this approach. Next, using the Singleton fuzzifier, product inference engine and center average defuzzifier, the three fuzzy systems are formed as (34)-(36):

$$K_p'(t) = \frac{\sum_{l=1}^{49} \bar{y}_p^l \mu_{A^l}(e(t)) \mu_{B^l}(\dot{e}(t))}{\sum_{l=1}^{49} \mu_{A^l}(e(t)) \mu_{B^l}(\dot{e}(t))} \quad (34)$$

$$K_d'(t) = \frac{\sum_{l=1}^{49} \bar{y}_d^l \mu_{A^l}(e(t)) \mu_{B^l}(\dot{e}(t))}{\sum_{l=1}^{49} \mu_{A^l}(e(t)) \mu_{B^l}(\dot{e}(t))} \quad (35)$$

$$\alpha(t) = \frac{\sum_{l=1}^{49} \bar{y}_\alpha^l \mu_{A^l}(e(t)) \mu_{B^l}(\dot{e}(t))}{\sum_{l=1}^{49} \mu_{A^l}(e(t)) \mu_{B^l}(\dot{e}(t))} \quad (36)$$

Where A^l and B^l are shown in Figure 4, and $\bar{y}_p^l$, $\bar{y}_d^l$ and $\bar{y}_\alpha^l$ are the center of the corresponding fuzzy sets shown in Figures 5-6. Figures 7-9 depict the corresponding output diagrams of these fuzzy systems.

[Downloaded from ijrare.iust.ac.ir on 2026-11-16]

[DOI: 10.22068/IJRARE.4.2.41]

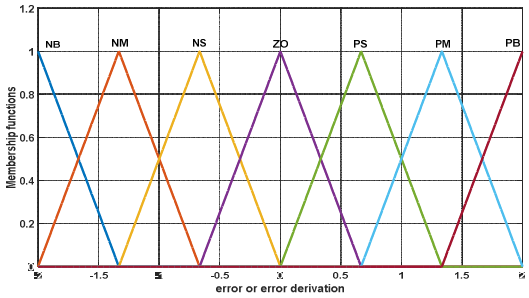

Figure 4. The membership functions defined in the variation ranges of the input signals (error and error derivation)

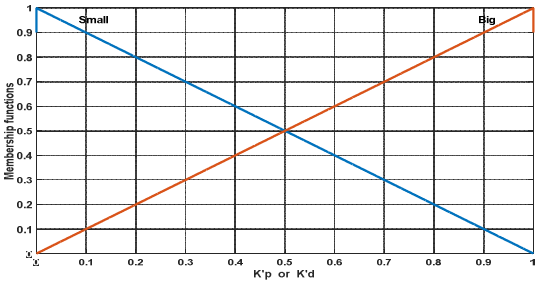

Figure 5. The membership functions defined in the variation ranges of $K_p^{'}$ and $K_d^{'}$

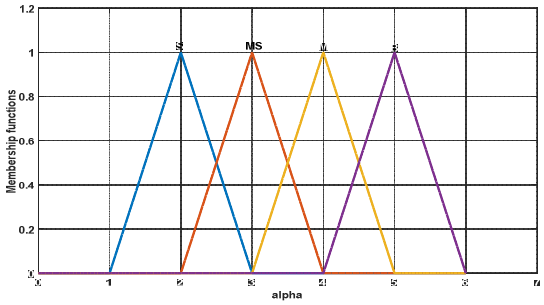

Figure 6. The membership functions defined in the variation range of α

Table 2. Fuzzy rule base for $K_p^{'}$

		e·(t)						
		NB	NM	NS	ZO	PS	PM	PB
e(t)	NB	B	B	B	B	B	B	B
	NM	S	B	B	B	B	B	S
	NS	S	S	B	B	B	S	S
	ZO	S	S	S	B	S	S	S
	PS	S	S	B	B	B	S	S
	PM	S	B	B	B	B	B	S
	PB	B	B	B	B	B	B	B

Table 3. Fuzzy rule base for $K_d^{'}$

		e·(t)						
		NB	NM	NS	ZO	PS	PM	PB
e(t)	NB	S	S	S	S	S	S	S
	NM	B	B	S	S	S	B	B
	NS	B	B	B	S	B	B	B
	ZO	B	B	B	B	B	B	B
	PS	B	B	B	S	B	B	B
	PM	B	B	S	S	S	B	B
	PB	S	S	S	S	S	S	S

Table 4. Fuzzy rule base for α

		e·(t)						
		NB	NM	NS	ZO	PS	PM	PB
e(t)	NB	2	2	2	2	2	2	2
	NM	3	3	2	2	2	3	3
	NS	4	3	3	2	3	3	4
	ZO	5	4	3	3	3	4	5
	PS	4	3	3	2	3	3	4
	PM	3	3	2	2	2	3	3
	PB	2	2	2	2	2	2	2

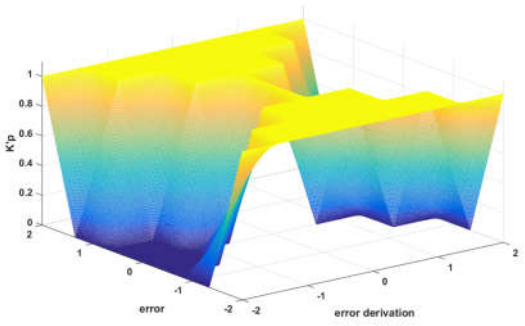

Figure 7. The output diagram of $K_p^{'}$

[Downloaded from ijrare.iust.ac.ir on 2026-11-16]

[DOI: 10.22068/IJRARE.4.2.41]

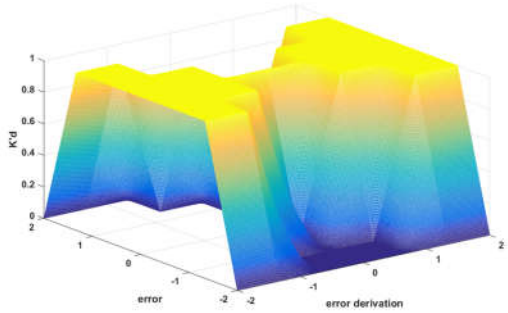

Figure 8. The output diagram of $K_d^{'}$

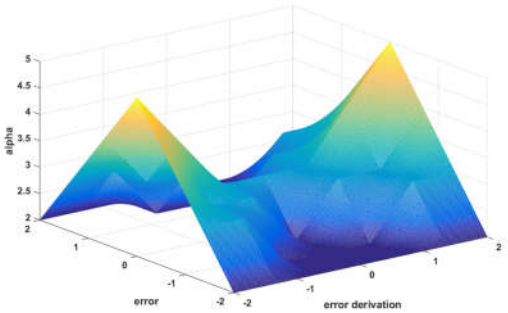

Figure 9. The output diagram of α

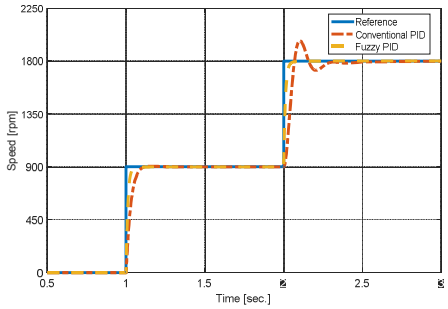

Figure 10. Performance comparison of the conventional PID and fuzzy PID controllers

In order to make a better comparison between the performances of the conventional PID and the used Fuzzy PID controllers, a step reference speed waveform as shown in Figure 10 is applied to a PMSM. Note that the motor is the same one that was used in the simulation section. As shown in this Figure, the performance achieved using the conventional PID controller with constant parameters won't be optimized anymore after the motor parameters are changed by 10 percent at t=1.5s. But, the fuzzy PID controller shows a satisfactory performance in all conditions.

6. Simulation Results

In order to evaluate and verify the performance of the inverter that is used and also the suggested control scheme for traction applications, the system is simulated in the MATLAB/Simulink environment. The parameters used in this simulation are shown in Table 5.

In the conducted simulation, a special reference speed for traction applications is considered. This reference speed waveform has five different modes including: (a) rheostatic acceleration (from $t=0$ to $t=5s$), (b) speed curve running (from $t=5s$ to $t=15s$), (c) free running (from $t=15s$ to $t=50s$), (d) coasting (from $t=50s$ to $t=57s$), (e) braking (from $t=57s$ to $t=60s$).

Table 5. Simulation parameters

Parameter	Value
Switching Frequency	1260 Hz
DC Link Voltage	780 V
Stator Resistance	0.05 Ω
Stator Inductance	63.5 mH
PM Flux	0.192 V.s

The waveforms of the reference and also the actual motor speeds are shown in Figure 11. In this Figure, for each of the 5 aforementioned modes, the diagram is enlarged and the reference and actual speeds are compared with each other. As seen in this figure, the actual speed includes only a very small error compared to its reference in rheostatic acceleration, speed curve running, coasting and braking modes (the maximum value of this error is 5 rpm). In the free running mode, the motor actual speed only consists of a small ripple component around the reference speed value. The maximum magnitude of this ripple doesn't exceed 0.5 rpm in this case. The above analysis reveals that the proposed control method has the ability to track the speed reference very well for railway applications. Also, the advantage of using the fuzzy PID supervisory control in comparison with the conventional PID controller is obvious according to the results. Using the suggested fuzzy PID controller results in satisfactory

[Downloaded from ijrare.iust.ac.ir on 2026-11-16]

[DOI: 10.22068/IJRARE.4.2.41]

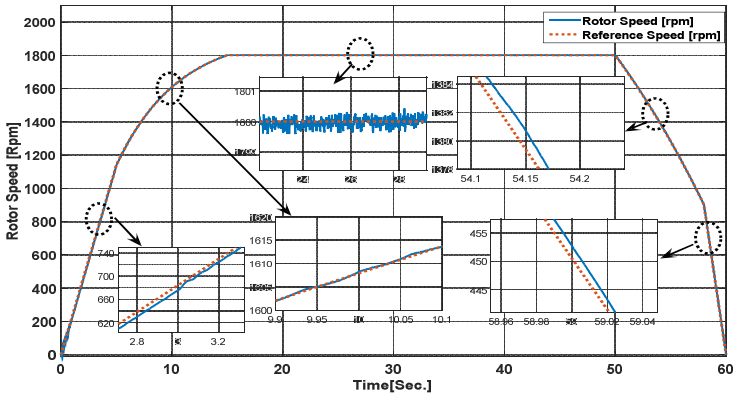

Figure 11. The reference and actual speeds of the PMSM for traction applications

dynamic and steady state performances for all the modes.

Figure 12 depicts the reference and actual waveforms of the q-axis component of the stator current (i_{sq}). As it is obvious, this current tracks its reference appropriately. However, the actual current includes a small ripple component around the reference value. In the worst condition that occurs at the variable speed modes of the reference speed, the peak value of this ripple is lower than 10 percent of the reference value. In the free running mode, this amount is much smaller (less than 4% of the reference value).

Figure 13 shows the reference and actual waveforms of the stator current d-axis component (i_{sd}). It should be noted that as described before, the reference value of i_{sd} is kept zero in the control strategy used through this paper. However, the actual value of this current has a negligible ripple component around its reference.

Figure 14 depicts the electromagnetic torque produced by the PMSM during its operation in different modes. As it is mentioned in the previous sections of the paper, the electromagnetic torque is proportional to the q-axis current (i_{sq}) because the reference value of i_{sd} is kept at zero. In the acceleration and constant speed modes of the reference speed waveform, the i_{sq} and T_e values are positive. In the free running mode, this positive value is slightly more than the load torque due to the presence of friction. In the modes after the free running interval, the torque reference is negative due to the braking performance. It can be seen that the generated electromagnetic torque tracks the reference very well by using the proposed strategy. Although there is a small ripple available in the generated torque waveform, but its maximum value is lower than 5 percent of the reference waveform in the worst case.

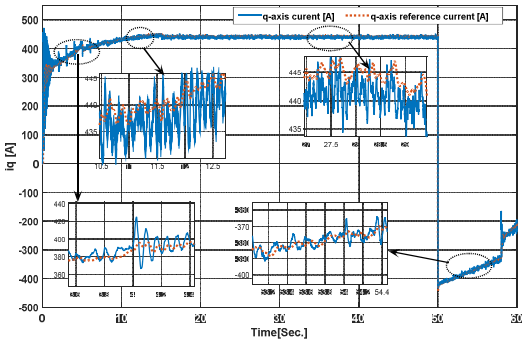

Figure 12. The reference and actual waveforms of the q-axis current i_{sq}

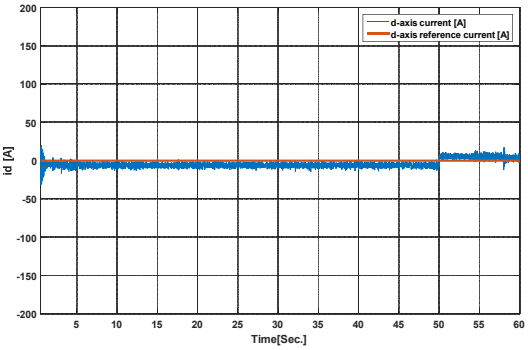

Figure 13. The reference and actual waveforms of the q-axis current i_{sd}

[Downloaded from ijrare.iust.ac.ir on 2026-11-16]

[DOI: 10.22068/IJRARE.4.2.41]

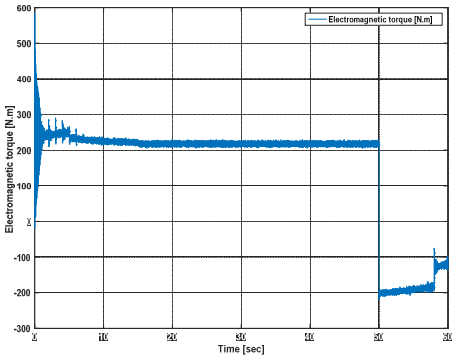

Figure 14. The electromagnetic torque produced by the PMSM

In Figures 15-19, the different waveforms related to the SMC are shown for each mode available in the reference speed. Each figure includes the phase and line voltages of the motor (which are generated by the SMC), the input currents of the motor and also the per unit (p.u.) value of the reference voltages generated by the control scheme. As it is shown, the phase and line voltages of the PMSM are multilevel voltages produced by the SMC. The number of the both phase and line voltage levels are the same as in Table 1 and only the pulse width and frequency of these voltages are changed during different modes. This is because of the differences between the magnitude and frequency of the reference voltages for these modes. As the reference speed value increases, the main component frequency and magnitude of the reference voltage generated by the control system is increased, as well.

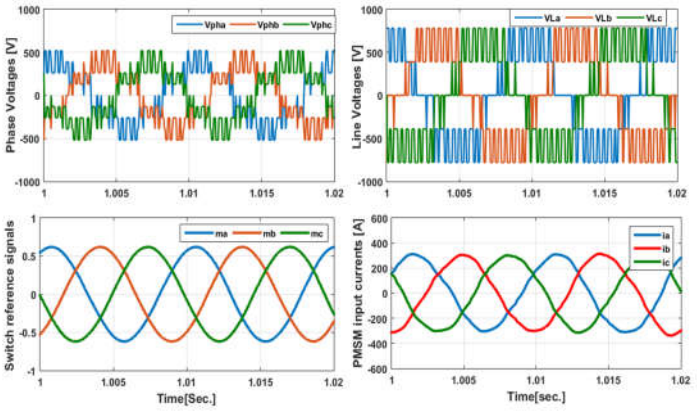

Figure 15. SMC waveforms for rheostatic acceleration mode,
(a) phase voltages, (b) line voltages, (c) amplitude modulation index, (d) PMSM input currents

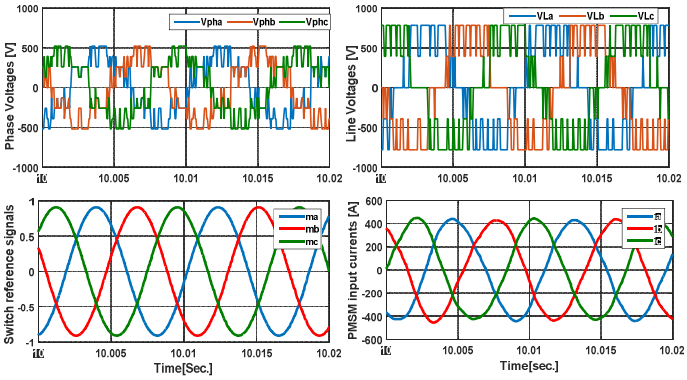

Figure 16. SMC waveforms for speed curve running mode,
(a) phase voltages, (b) line voltages, (c) amplitude modulation index, (d) PMSM input currents

[Downloaded from ijrare.iust.ac.ir on 2026-11-16]

[DOI: 10.22068/IJRARE.4.2.41]

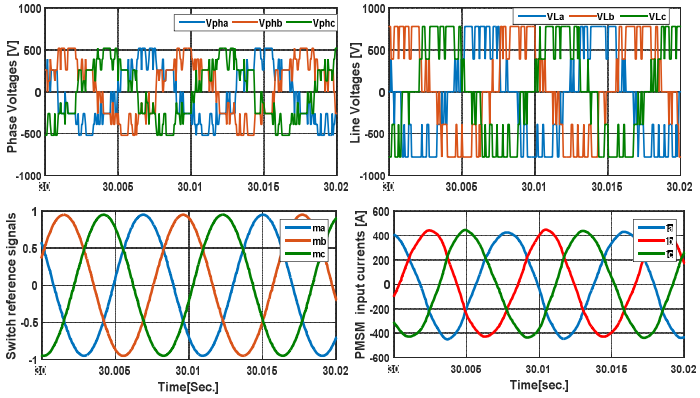

Figure 17. SMC waveforms for free running mode,
(a) phase voltages, (b) line voltages, (c) amplitude modulation index, (d) PMSM input currents

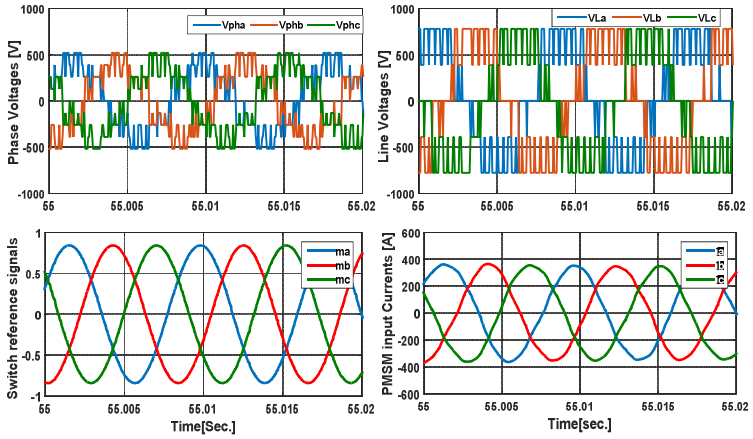

Figure 18. SMC waveforms for coasting mode,
(a) phase voltages, (b) line voltages, (c) amplitude modulation index, (d) PMSM input currents

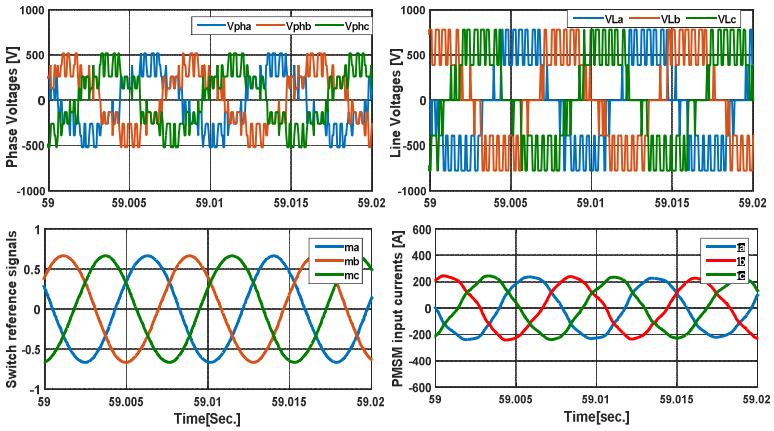

Figure 19. SMC waveforms for braking mode,
(a) phase voltages, (b) line voltages, (c) amplitude modulation index, (d) PMSM input currents

[Downloaded from ijrare.iust.ac.ir on 2026-11-16]

[DOI: 10.22068/IJRARE.4.2.41]

Moreover, the current waveforms are sinusoidal ones with very low THD values (lower than 4.7% for all conditions). In lower speeds, the current THD values are more and as the speed increases, the THD value improves. The harmonic content of the current waveforms are due to the ripple components of i_{ds} and i_{qs}. However, it should be noted that these ripple components and the harmonic content of the currents as a result, are lower than the same values for conventional inverters due to the use of SMC which is a multilevel converter. Also, the magnitude of the reference voltage waveforms in the p.u. system represents the amplitude modulation index (m_a) value. As it is obvious, the m_a value is less than 1 during the whole performance period and hence, the inverter doesn't reach the over-modulation mod.

7. Conclusion

In this paper, a PMSM-based drive system for railway traction applications is proposed. In this system, the FOC is used as the control strategy. Moreover, the inverter used in the system is a multilevel converter named SMC. Using the SMC converter results in the decrease of voltage THD value and therefore, providing a better power quality for the motor. Moreover, using fuzzy supervisory control for the conventional PID controller results in an improved dynamic performance with a smaller steady state error value for all different conditions. The conducted simulation results reveals the effectiveness and good performance of the proposed method in comparison with the conventional FOC strategy. According to the simulation results, the selected scheme provides acceptable torque ripple and THD values for traction applications also the reference speed tracking is accurate enough for this application.

References

[1] I. Bolvashenkov, J. Kammermann, and H.-G. Herzog, "Methodology for selecting electric traction motors and its application to vehicle propulsion systems," in Power Electronics, Electrical Drives, Automation and Motion (SPEEDAM), 2016 International Symposium on, (2016), pp. 1214-1219.

[2] S. Hillmansen, "Electric railway traction systems and techniques for energy saving," IET Professional Development Course on Electric Traction Systems, (2012), pp. 19-23.

[3] H. Douglas, F. Schmid, C. Roberts, and S. Hillmansen, "Evaluation of Permanent Magnet Motor energy saving technology for different types of railways," in Intelligent Rail Transportation (ICIRT), 2016 IEEE International Conference on, (2016), pp. 123-129.

[4] R. Saidur, S. Mekhilef, M. Ali, A. Safari, and H. Mohammed, "Applications of variable speed drive (VSD) in electrical motors energy savings," Renewable and Sustainable Energy Reviews, vol. 16, (2012), pp. 543-550.

[5] G. Pellegrino, A. Vagati, B. Boazzo, and P. Guglielmi, "Comparison of induction and PM synchronous motor drives for EV application including design examples," IEEE Transactions on industry applications, vol. 48, (2012), pp. 2322-2332.

[6] J. Wang, X. Yuan, and K. Atallah, "Design optimization of a surface-mounted permanent-magnet motor with concentrated windings for electric vehicle applications," IEEE Transactions on Vehicular Technology, vol. 62, (2013), pp. 1053-1064.

[7] K. Kamiev, J. Montonen, M.P. Ragavendra, J. Pyrhönen, J.A. Tapia, and M. Niemelä, "Design principles of permanent magnet synchronous machines for parallel hybrid or traction applications," IEEE Transactions on Industrial Electronics, vol. 60, (2013), pp. 4881-4890.

[8] H.-W. Lee, C.-B. Park, and B.-S. Lee, "Performance comparison of the railway traction IPM motors between concentrated winding and distributed winding," in Transportation Electrification Conference and Expo (ITEC), 2012 IEEE, (2012), pp. 1-4.

[9] J. Hu, W. Liu, and J. Yang, "Application of power electronic devices in rail transportation traction system," in Power Semiconductor Devices & IC's (ISPSD), 2015 IEEE 27th International Symposium on, (2015), pp. 7-12.

[10] J. Taufiq, "Power electronics technologies for railway vehicles," in Power Conversion Conference-Nagoya, 2007. PCC'07, (2007), pp. 1388-1393.

[11] F. Betin, G.-A. Capolino, D. Casadei, B. Kawkabani, R. I. Bojoi, L. Harnefors, E. Levi, L. Parsa, and B. Fahimi, "Trends in electrical

[Downloaded from ijrare.iust.ac.ir on 2026-11-16]

[DOI: 10.22068/IJRARE.4.2.41]

machines control: Samples for classical, sensorless, and fault-tolerant techniques," IEEE Industrial Electronics Magazine, vol. 8, (2014), pp. 43-55.

[12] J. Simanek, J. Novak, R. Dolecek, and O. Cerny, "Control algorithms for permanent magnet synchronous traction motor," in EUROCON, 2007. The International Conference on" Computer as a Tool", (2007), pp. 1839-1844.

[13] S. Zhao, X. Huang, Y. Fang, and J. Li, "A control scheme for a High Speed Railway traction system based on high power PMSM," in Power Electronics Systems and Applications (PESA), 2015 6th International Conference on, (2015), pp. 1-8.

[14] W. Wang, M. Cheng, B. Zhang, Y. Zhu, and S. Ding, "A fault-tolerant permanent-magnet traction module for subway applications," IEEE Transactions on Power Electronics, vol. 29, (2014), pp. 1646-1658.

[15] S.S. Fazel, M. Khorshidi, and M. Niakinezhad, "Investigation of SLIM Dynamic Models Based on Vector Control for Railway Applications," Advances in Railway Engineering,An International Journal, vol. 2, (2014), pp. 85-92.

[16] X. del Toro Garcia, B. Zigmund, A.A. Terlizzi, R. Pavlanin, and L. Salvatore, "Comparison between FOC and DTC strategies for permanent magnet synchronous motors," Advances in Electrical and Electronic Engineering, vol. 5, (2006), p. 76.

[17] R. Bojoi, M. Pastorelli, J. Bottomley, P. Giangrande, and C. Gerada, "Sensorless control of PM motor drives—A technology status review," in Electrical Machines Design Control and Diagnosis (WEMDCD), 2013 IEEE Workshop on, (2013), pp. 168-182.

[18] K. Kondo, "PMSM and IM rotational sensorless technologies specialized for railway vehicles traction," in Sensorless Control for Electrical Drives (SLED), 2014 IEEE 5th International Symposium on, (2014), pp. 1-7.

[19] O. Wallmark, J. Galic, M. Jansson, and H. Mosskull, "A robust sensorless control scheme for permanent-magnet motors in railway traction applications," in Electrical Systems for Aircraft, Railway and Ship Propulsion (ESARS), 2012, (2012), pp. 1-5.

[20] E. Baser and Y. Altun, "The estimation of PID controller parameters of vector controlled induction motor using Ziegler-Nichols method," Journal of Engineering Research and Applied Science, vol. 4, (2015), pp. 278-282.

[21] Y. Wu, B. Jiang, and P. Shi, "Incipient fault diagnosis for T–S fuzzy systems with application to high-speed railway traction devices," IET Control Theory & Applications, vol. 10, (2016), pp. 2286-2297.

[22] K. Noori and K. Jenab, "Fuzzy reliability-based traction control model for intelligent transportation systems," IEEE Transactions on Systems, Man, and Cybernetics: Systems, vol. 43, (2013), pp. 229-234.

[23] A. Mishra, V. Mahajan, P. Agarwal, and S. Srivastava, "Fuzzy logic based speed and current control of vector controlled PMSM drive," in Power, Control and Embedded Systems (ICPCES), 2012 2nd International Conference on, (2012), pp. 1-6.

[24] B. Roy, and S. Sisodiya, "Fuzzy logic controller based speed analysis and control of DC shunt motor, " IJRASET, vol. 3(X), (2015), pp. 152-157.

[25] G. Singh and G. Singh, "A fuzzy pre-compensated-PI controller for indirect field oriented controlled induction motor drive," in Computational Intelligence on Power, Energy and Controls with their impact on Humanity (CIPECH), 2014 Innovative Applications of, (2014), pp. 257-261.

[26] M.R. Hazari, E. Jahan, M.A. Mannan, and J. Tamura, "Design and simulation of fuzzy logic based speed control for an SVPWM inverter-fed induction motor considering core loss and stray load losses," in Electrical and Computer Engineering (WIECON-ECE), 2015 IEEE International WIE Conference on, (2015), pp. 5-9.

[27] A.M. El-Refaie, "Motors/generators for traction/propulsion applications: A review," IEEE Vehicular Technology Magazine, vol. 8, (2013), pp. 90-99.

[28] J. Ren, H. Feng, H. Ren, and Y. Huang, "Simulation of PMSM vector control system based on propeller load characteristic," in Intelligent Control and Information Processing (ICICIP), 2010 International Conference on, (2010), pp. 735-737.

[Downloaded from ijrare.iust.ac.ir on 2026-11-16]

[DOI: 10.22068/IJRARE.4.2.41]

[29] S. M. M. Sangdehi, S. Hamidifar, and N. C. Kar, "A novel bidirectional DC/AC stacked matrix converter design for electrified vehicle applications," IEEE Transactions on Vehicular Technology, vol. 63, (2014), pp. 3038-3050.

[30] L.-X. Wang, A course in fuzzy systems: Prentice-Hall press, USA, 1999.

[Downloaded from ijrare.iust.ac.ir on 2026-11-16]

[DOI: 10.22068/IJRARE.4.2.41]